Cosine-Sine Modulated Filter Banks for Motion Estimation and Correction

Marco Maass(✉), Huy Phan, Anita Möller, and Alfred Mertins

Institute for Signal Processing, University of Lübeck, 23562 Lübeck, Germany
{maass,phan,moeller,mertins}@isip.uni-luebeck.de

Abstract. We present a new motion estimation algorithm that uses cosine-sine modulated filter banks to form complex modulated filter banks. The motion estimation is based on phase differences between a template and the reference image. By using a non-downsampled version of the cosine-sine modulated filter bank, our algorithm is able to shift the template image over the reference image in the transform domain by only changing the phases of the template image based on a given motion field. We also show that we can correct small non-rigid motions by directly using the phase difference between the reference and the template images in the transform domain. We also include a first application in magnetic resonance imaging, where the Fourier space is corrupted by motion and we use the phase difference method to correct small motion. This indicates the magnitude invariance for small motions.

Keywords: Motion estimation · Motion correction · Motion invariance · Cosine-sine modulated filter banks · Motion mri

1 Introduction

In the literature, different methods have been proposed for motion field estimation. They can be grouped into direct and indirect methods. For direct methods, block-matching algorithms [9] are most intuitive and traditional. In these algorithms, the template image is splitted into blocks each of which is then used to search the best matching block in the reference image to measure the shift of that block. Methods for capturing the real motion more efficiently are based on optical flow models [6]. With the assumption that the brightness of an image $I(x, y, t)$ at (x, y) is changed only due to the temporal motion, the motion field can be estimated under the assumption of a constant overall brightness [6], in which the total time derivative is constrained to be zero. Indirect methods, on the other hand, utilize different kinds of features and edge detection techniques to estimate the motion field [15]. An overview of different techniques can be found in [13].

Motion estimation can be done in the subband domain of filter banks based on special filter design techniques [4,11]. These methods rely on the principle that a shift in the spatial domain only causes a phase change in the subband

S. Battiato et al. (Eds.): ACIVS 2015, LNCS 9386, pp. 195–204, 2015.
DOI: 10.1007/978-3-319-25903-1_17

domain, and the magnitude is not influenced. In [4], the motion estimation was performed using the complex bandpass Gabor filters which are optimally located in spatial and frequency space. This was then extended in [11] to develop a hierarchical estimation algorithm by using dyadic complex discrete wavelets transform (ℂ-DWT).

It has been shown that a so-called dual-tree complex wavelet transform (DT-ℂ-DWT) can be used as ℂ-DWT [14]. The idea behind the DT-ℂ-DWT is that instead of directly using a ℂ-DWT, we can perform two real-valued normal discrete wavelet transforms (DWT). This is possible if two real-valued filter pairs $\{h_0(n), h_1(n)\}$ and $\{\tilde{h}_0(n), \tilde{h}_1(n)\}$ from the first and second DWT respectively are designed as Hilbert-transform pairs. Then, the complex summation of the first and second filter bank results in a ℂ-DWT [14]. The DT-ℂ-DWT theory was further extended to uniform M-band filter banks [3] and different design methods have been proposed based on this extension [3,2,8].

Our proposed method in this work relies on filter design techniques for cosine-sine modulated filter banks. We employ the M-band DT-ℂ-DWT without DC-leakage proposed in our previous work [10]. The DC-leakage-free property of filter banks is important in image processing to avoid corrupting the higher-order bandpass filtered images by their DC components. The M-band DT-ℂ-DWT was first proposed in [16] in form of a cosine-sine modulated filter bank (CSMFB). The idea behind modulated filter banks is to derive all subband filters from a single real-valued prototype. It was shown that the CSMFB can be interpreted as an M-band DT-ℂ-DWT [8], where the cosine and sine modulated filter banks, respectively, correspond to the real and the imaginary part of the ℂ-DWT. This is illustrated in Fig. 1. In [10], we improved CSMFB to obtain DC-leakage-free property by introducing a lifting factorization to design prototype filters. We will show that, by using the M-band DT-ℂ-DWT without DC-leakage, the coefficient magnitudes are invariant to small motion, and most information about the motion between neighboring frames is contained in the phase differences only. Furthermore, it can be also used for motion estimation and correction with applications in video processing and magnetic resonance imaging.

2 Cosine-Sine Modulated Filter Bank

The one-dimensional CSMFB, illustrated in Fig. 1, has two M-band filter banks, each of which is decimated by N. The system functions $H_k(z)$, $\tilde{H}_k(z)$, $F_k(z)$ and $\tilde{F}_k(z)$ are expressed as cosine- and sine-modulated version of the real-valued prototype $P(z)$ [17]. As proved in [8], the filter bank can also be seen as an M-band DT-ℂ-DWT. The one-dimensional complex analysis filters are obtained by

$$\begin{aligned} G_k(z) &= H_k(z) + j\tilde{H}_k(z) \\ G_k^*(z) &= H_k(z) - j\tilde{H}_k(z) \end{aligned} \tag{1}$$

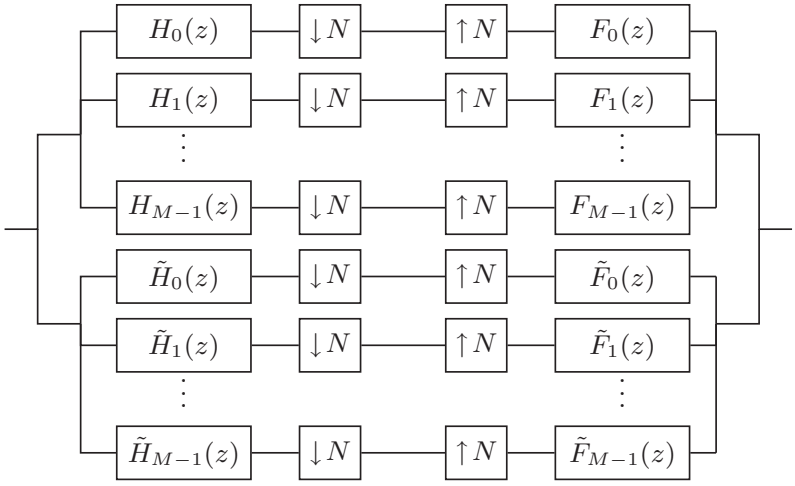

Fig. 1. M-band dual-tree wavelet transform and cosine-sine modulated filter bank.

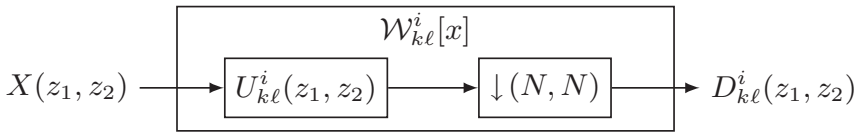

Fig. 2. Processing the image $x(n, m)$ with the transform $\mathcal{W}^i_{k\ell}[x]$ which consists of the complex bandpass filter $u^i_{k\ell}(n, m)$ followed by the downsampler $\downarrow (N, N)$.

with $H_k(z)$ and $\tilde{H}_k(z)$ defined in [10]. For motion estimation, we need the central frequencies of $G_k(e^{j\omega})$ and $G^*_k(e^{j\omega})$. Under the assumption

$$\left(\operatorname*{argmax}_{\omega} \left| P(e^{j\omega}) \right| \right) = 0, \tag{2}$$

it can be easily verified that the central frequency for $G_k(e^{j\omega})$ is

$$\omega_k = \operatorname*{argmax}_{\omega} \left| G_k(e^{j\omega}) \right| = \left(k + \frac{1}{2} \right) \frac{\pi}{M}. \tag{3}$$

The central frequency ω^*_k for $G^*_k(e^{j\omega})$ can equivalently be calculated.

Following the standard approach [14] for DT-ℂ-DWT, extensions to a two-dimensional M-band DT-ℂ-DWT can be found in the literature [3,7]. For image filtering, the two-dimensional complex bandpass filter will compose two separable bandpass filters, one filter on the columns and the other on the rows. They are defined as

$$\begin{aligned} U^1_{k\ell}(z_1, z_2) &= \left(U^4_{k\ell}(z_1, z_2) \right)^* = G_k(z_1) G_\ell(z_2) \\ U^2_{k\ell}(z_1, z_2) &= \left(U^3_{k\ell}(z_1, z_2) \right)^* = G_k(z_1) G^*_\ell(z_2). \end{aligned} \tag{4}$$

As a consequence, $2M$ filters in one dimension result in $4 \cdot (M \times M)$ two-dimensional bandpass filters. The filtering process on an image $x(n, m)$ with a complex filter $u^i_{k\ell}(n, m)$ is illustrated in Fig. 2.

Complex filters can be completely shift invariant if they have a compact support on one half of the frequency space. However, this can only be achieved with

IIR filters [14]. Therefore, we have to accept that we can only obtain approximate shift invariance for DT-ℂ-DWT. Fortunately, we will show that, for the CSMFB we can arbitrarily choose the number of subbands, and the higher number of bands should produce more shift invariance.

The shift invariance property can be defined by processing an image $x(\boldsymbol{n}) = x(n,m)$ and its shifted version $\hat{x}(\boldsymbol{n}) = x(\boldsymbol{n}+\boldsymbol{s}) = x(n+s_1(\boldsymbol{n}), m+s_2(\boldsymbol{n}))$ with the transform $\mathcal{W}^i_{k\ell}[x]$. $\mathcal{W}^i_{k\ell}[x]$, as in Fig. 2, consists of the complex bandpass filter $u^i_{k\ell}(n,m)$ followed by the downsampler $\downarrow(N,N)$. The shift invariance can be described as

$$\begin{aligned}\mathcal{W}^1_{k\ell}[\hat{x}(\boldsymbol{n})] &\approx e^{j(\omega_k \tilde{s}_1(\boldsymbol{m})+\omega_\ell \tilde{s}_2(\boldsymbol{m}))}\mathcal{W}^1_{k\ell}[x(\boldsymbol{n})],\\ \mathcal{W}^2_{k\ell}[\hat{x}(\boldsymbol{n})] &\approx e^{j(\omega_k \tilde{s}_1(\boldsymbol{m})+\omega^*_\ell \tilde{s}_2(\boldsymbol{m}))}\mathcal{W}^2_{k\ell}[x(\boldsymbol{n})],\end{aligned} \tag{5}$$

where ω_k, ω_ℓ and ω^*_ℓ are defined by (3) and $\tilde{s}_i(\boldsymbol{m}) = s_i(N\boldsymbol{m})$ is the downsampled shift. This means that the difference between $x(n,m)$ and $\hat{x}(n,m)$ can be approximated by only a phase shift in the transform domain, while the magnitudes remain approximately equal.

3 Motion Estimation

3.1 The Error Function

Based on the work in [11], we develop a motion estimation algorithm using the CSMFB. The idea of this algorithm is to obtain the approximate shift invariance on the subband images, as in (5). Let $x(\boldsymbol{n})$ denote the reference image and $\hat{x}(\boldsymbol{n}) \approx x(\boldsymbol{n}+\boldsymbol{s})$ denote the current image, respectively. The subband error can be defined as

$$\begin{aligned}\mathcal{E}^i_{k\ell}(\boldsymbol{n},\boldsymbol{s}) \approx{}& \left(\left|\mathcal{W}^i_{k\ell}[x(\boldsymbol{n})]\right| - \left|\mathcal{W}^i_{k\ell}[\hat{x}(\boldsymbol{n})]\right|\right)^2\\ &+ \left|\mathcal{W}^i_{k\ell}[x(\boldsymbol{n})]\mathcal{W}^i_{k\ell}[\hat{x}(\boldsymbol{n})]\right| \cdot \left\{ \left[\boldsymbol{\Omega}^i_{k\ell}\right]^T \tilde{\boldsymbol{s}}(\boldsymbol{m}) - \theta^i_{k\ell}(\boldsymbol{m}) \right\},\end{aligned} \tag{6}$$

where $\mathcal{W}^i_{k\ell}[\boldsymbol{x}]$ represents the subfilter bank as in Fig. 2 and

$$\begin{aligned}\theta^i_{kl}(\boldsymbol{m}) &= \angle\left[\frac{\mathcal{W}^i_{k\ell}[\hat{x}(\boldsymbol{n})]}{\mathcal{W}^i_{k\ell}[x(\boldsymbol{n})]}\right], \quad \tilde{\boldsymbol{s}}(\boldsymbol{m}) = [\tilde{s}_1(\boldsymbol{m}), \tilde{s}_2(\boldsymbol{m})]^T,\\ \boldsymbol{\Omega}^1_{k\ell} &= [\omega_k, \omega_\ell]^T, \quad \text{and} \quad \boldsymbol{\Omega}^2_{kl} = [\omega_k, \omega^*_\ell]^T.\end{aligned} \tag{7}$$

Note that in our case the scale of the last quadratic term in (6) is different from that in [11] since on each level M of the motion estimation the transform produces subbands in the complete frequency space. Normally, the images are real-valued, therefore the motion estimation will only be performed on $i = 1, 2$ as formulated in (7). The complete error function for the level M is then determined by

$$\mathcal{E}(\boldsymbol{n},\boldsymbol{s}) = \sum_i \sum_{k,\ell=1}^{M-2} \mathcal{E}^i_{k\ell}(\boldsymbol{n},\boldsymbol{s}). \tag{8}$$

Here, we do not include the suberrors with $k, \ell \in \{0, M-1\}$, because these bands lap into the other frequency quadrants and the shift invariance is not valid anymore.

The combined error is a quadratic function and can be written as

$$\mathcal{E}(\boldsymbol{n}, \boldsymbol{s}) = A\tilde{s}_1^2 + B\tilde{s}_2^2 + C\tilde{s}_1\tilde{s}_2 + D\tilde{s}_1 + E\tilde{s}_2 + G. \tag{9}$$

3.2 Hierarchical Motion Estimation with CSMFB

Our hierarchical motion estimation approach starts with the level $M_{\max} = 2^{J_{\max}}$ and ends with the level $M_{\min} = 2^{J_{\min}}$. Here, M in $\mathcal{W}_{k\ell}^{(i,M)}[\boldsymbol{x}]$ represents both the number of bands and the downsampler in the CSMFB. The algorithm can also include prior knowledge about the motion field $\boldsymbol{s_0}(\boldsymbol{n})$ and has the following steps:

1. Perform the transformation $\mathcal{W}_{k\ell}^{(i,M)}[x]$ for the reference frame $x(\boldsymbol{n})$ and the current frame $\hat{x}(\boldsymbol{n})$ for each level $M = 2^J$ with $J = J_{\min}, \ldots, J_{\max}$ and each subband i, k and ℓ. If the image is real-valued, it is sufficient to perform the transformation only for $i = 1, 2$.
2. For each level M from $M_{\max}$ to $M_{\min}$
   - If there is prior knowledge about the motion included, correct motion on the downsampled grid $\tilde{\boldsymbol{s}}_{\boldsymbol{0}}(\boldsymbol{m})$ for all subbands $\mathcal{W}_{k\ell}^{(i,M)}[x(\boldsymbol{n})]$ with (5).
   - Calculate $\Delta\tilde{\boldsymbol{s}}_{\boldsymbol{0}}(\boldsymbol{m}) = \operatorname{argmin}_{\boldsymbol{s}} \mathcal{E}(\boldsymbol{n}, \boldsymbol{s})$ by (9).
   - Interpolate $\tilde{\boldsymbol{s}}_{\boldsymbol{0}}(\boldsymbol{m}) + \Delta\tilde{\boldsymbol{s}}_{\boldsymbol{0}}(\boldsymbol{m})$ to the next higher level.
   - If there exists prior knowledge about the motion on the higher level, use the mean of the prior motion and the interpolated motion as new prior motion $\tilde{\boldsymbol{s}}_{\boldsymbol{0}}(\boldsymbol{m})$.
3. Interpolate $\tilde{\boldsymbol{s}}_{\boldsymbol{0}}(\boldsymbol{m})$ from the last level to $\boldsymbol{s_0}(\boldsymbol{n})$ with the size of $x(\boldsymbol{n})$.
4. Repeat the algorithm with prior motion knowledge $\boldsymbol{s_0}(\boldsymbol{n})$ if necessary.

4 Results

4.1 Motion Estimation

To demonstrate the motion estimation properties of our algorithm under noisy conditions, we consider the Yosemite sequence without clouds, for which the ground truth motion is known[1]. The angular error measure is calculated as in [4]:

$$\psi_e = \arccos\left(\frac{\boldsymbol{v}^T\boldsymbol{v}^{coor}}{\|\boldsymbol{v}\| \cdot \|\boldsymbol{v}^{coor}\|}\right) \tag{10}$$

with $\boldsymbol{v} = [\boldsymbol{s}, 1]^T$ and $\boldsymbol{v}^{coor} = [\boldsymbol{s}^{coor}, 1]^T$. Here, $\boldsymbol{s}$ is the estimated motion vector and $\boldsymbol{s}^{coor}$ is the ground truth motion vector for one spatial position in the image. We calculated the mean $\overline{\psi}_e$ and the standard deviation σ_{ψ_e} of the angular error measures over the whole sequence.

In the estimation algorithm, we set the maximum level to $J_{\max} = 8$ and the minimum level to $J_{\min} = 4$. The frames were extended by zeros at the borders during the downsampling process. When calculating the mean and standard deviation, we took into account only pixel elements that are not in the cloud area of the image. We considered white Gaussian noise with zero mean and different standard deviations σ_g before processing the frames to check the robustness of our algorithm.

The experimental results on the angular error measure are shown in Table 1. As expected, the motion estimation for the noise-free case is relatively good, but it gets worse in noisy conditions. Although the performance of our system in terms of angular error measure is marginally lower than for the best algorithms in [1], it has some significant advantages with regard to motion correction. Our transform has similar properties as the Fourier transform in the sense of shift invariance of the magnitude. With the information being coded in the phase, we can directly calculate the motion field. In contrast to the Fourier transform, our method is able to cope with non-rigid motion and its associated noise.

Table 1. Mean and standard deviation for different noise level of the motion estimation

σ_g	0	10	20	30	40
$\overline{\psi}_e$	4.256°	11.642°	17.912°	24.463°	30.216°
σ_{ψ_e}	5.096°	10.596°	13.654°	18.074°	21.532°

4.2 Motion Correction

In this experiment, we perform motion correction between two frames by using the ground truth motion field of the Yosemite sequence without clouds and the filter bank without downsampling step. The downsampling step is not performed because the ground truth motion field can be directly applied by (5) to correct the bandpass filtered images. We used all subbands of the image excluding $\mathcal{W}^1_{0,0}[\boldsymbol{x}]$ and $\mathcal{W}^2_{0,0}[\boldsymbol{x}]$, because they include the DC-component of the image, and correcting the phase here can result in changing the image DC. The other bands do not include DC, because we used filters without DC-leakage [10].

After the correction, we transform the images back into the spatial domain. We measure the error of the correction as $\mathrm{E} = \|X_1 - X_2^{\mathrm{COOR}}\|_{\mathrm{F}}$, where X_1 denotes the reference frame and X_2^{COOR} denotes the corrected frame. By using the Frobenius norm $\|\cdot\|_{\mathrm{F}}$, we measure the distance between two images. As baseline we also include the error $\|X_1 - X_2\|_{\mathrm{F}}$, where X_2 is the next frame without motion correction. For this experiment, we normalized the pixel values to be in the interval $[0, 1]$. In Fig. 3, we show the error measures between neighboring frames. It can clearly be seen that it is possible to correct motion with a two-dimensional CSMFB for the given motion fields.

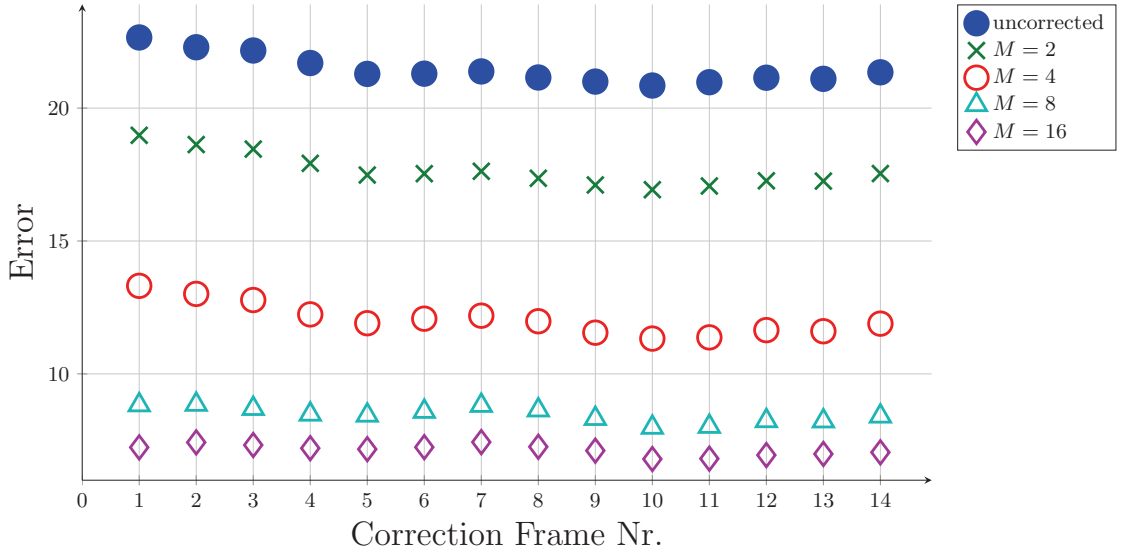

Fig. 3. Error of the motion correction using motion field correction with different number of bands $4M^2$ on the Yosemite sequence.

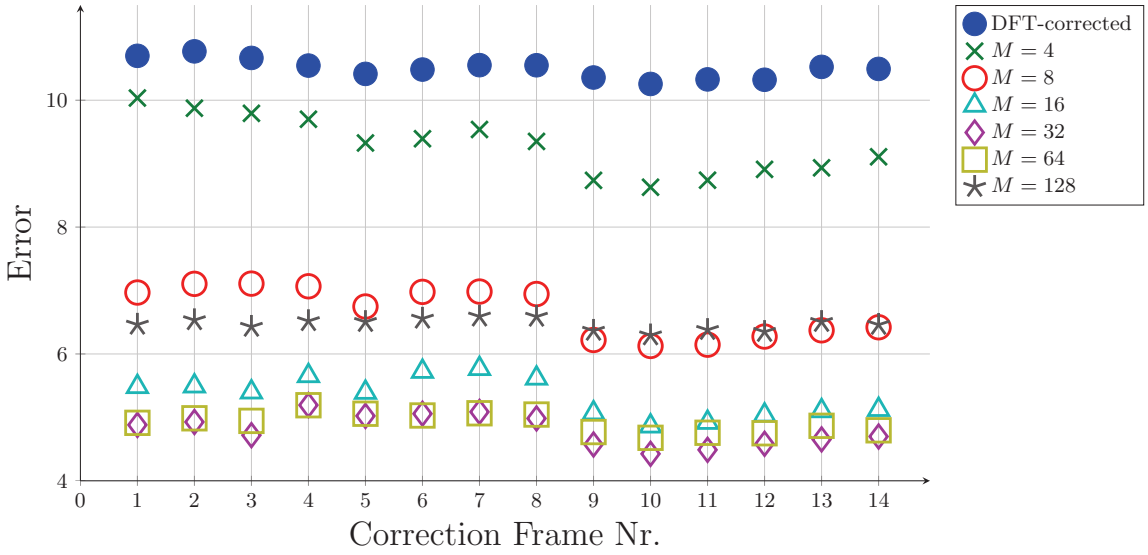

Fig. 4. Error of the motion correction using phase difference correction with different number of bands $4M^2$ on the Yosemite sequence.

4.3 Phase Shift Correction

In this experiment, we want to show that for a two-dimensional CSMFB with downsampling, the difference between the reference and the template frame is only in the phase differences of the subband images $\mathcal{W}^i_{k\ell}[\boldsymbol{x}]$. By correcting the phase differences, we are able to correct the non-rigid motion. As baseline, we used the Fourier transform which is optimal for correcting horizontal and vertical image shifts. In Fig. 4, we show the difference error between neighboring frames. Here, we used the Yosemite sequence with clouds, therefore we are not interested in the ground truth motion. As can be seen in Fig. 4, with increasing number of

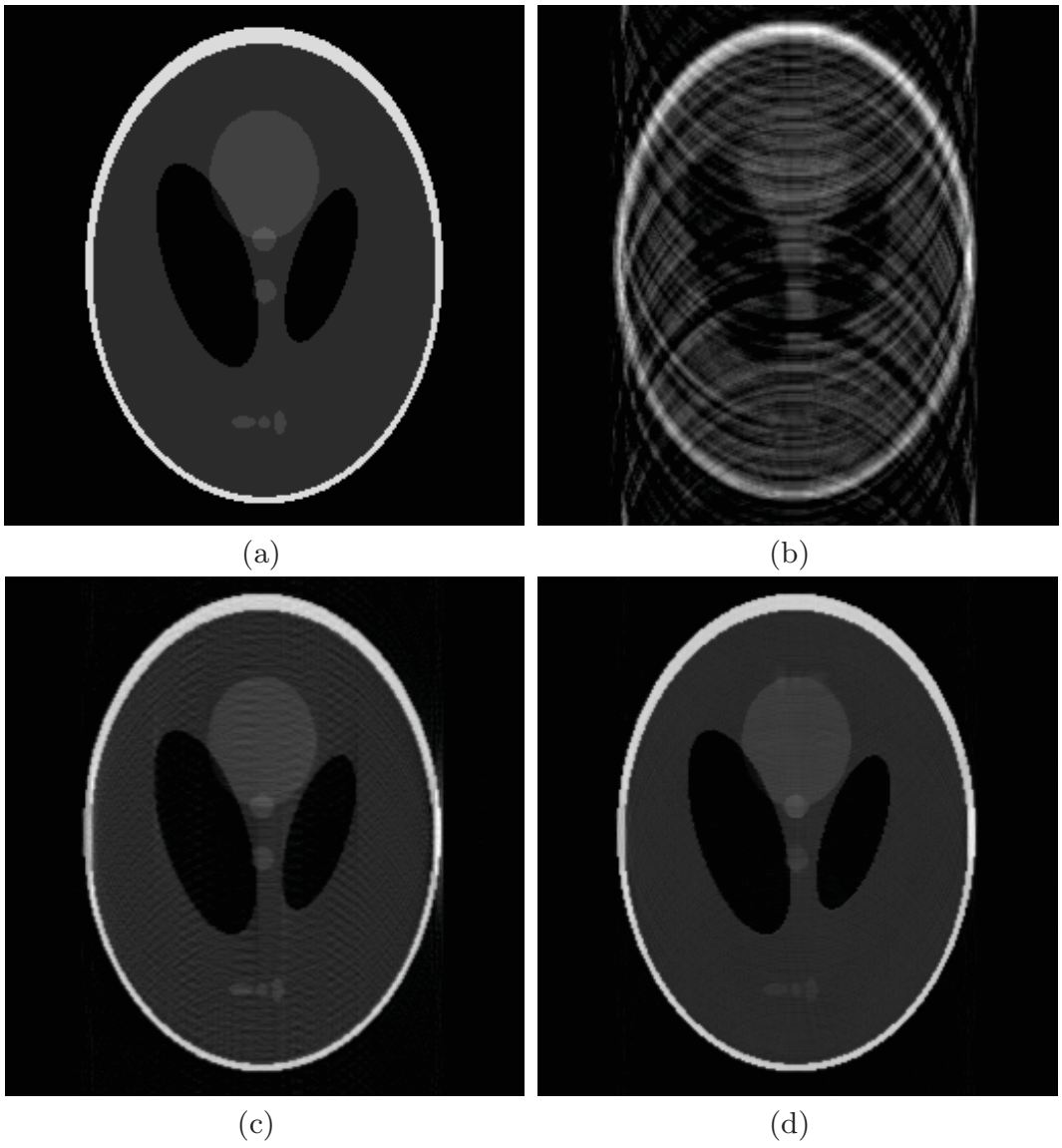

Fig. 5. Example of MR imaging. (a) Original. (b) The motion corrupted phantom. (c) The reconstruction by [12]. (d) The reconstruction with phase shift correction with $M = 16$.

bands, the motion correction becomes better until $M = 32$, which corresponds to $4 \cdot 32^2$ bandpass filtered images. With a reasonable number of bands, the motion information is coded only in the phase, and the motion can be easily corrected by the phase differences. For $M = 64$ and above, the motion correction becomes worse again. The reason is that a too large number of bands causes the two-dimensional CSMFB to become equivalent to the baseline Fourier transform.

4.4 Motion Correction in Magnetic Resonance Imaging

In magnetic resonance imaging the Fourier-space, called k-space, will be sampled directly. If the patient moves during the data acquisition, the movement will

result in motion artifacts after the reconstruction. Without any additional phase correction, the sampled medical images could be strongly corrupted by these motion artifacts, and diagnostics are not possible anymore. We extended the blind motion estimation in [18,12] for subpixel motion by a phase-correction step. We simulated the subpixel motion by linear interpolation on the Shepp-Logan phantom (256×256 pixels) by randomly chosen ± 5 pixel translational motion for each k-space line. The motion-corrupted image is denoted by $\boldsymbol{x}_m$. Then, we perform a first motion correction as in [12] to obtain the image $\boldsymbol{x}_s$. After that, we perform a total-variation denoising step with the algorithm in [5] and get the denoised image $\boldsymbol{x}_d$. Between all subbands $\mathcal{W}^i_{k\ell}[\boldsymbol{x}_d]$ and $\mathcal{W}^i_{k\ell}[\boldsymbol{x}_s]$, we calculate the phase differences in the transform-domain $\mathcal{W}$ by (5) and perform the correction for $\mathcal{W}^i_{k\ell}[\boldsymbol{x}_s]$. After the following inverse transform, we obtain the image $\tilde{\boldsymbol{x}}_s$. Finally, we used the Fourier-transform $\mathcal{F}[\hat{\boldsymbol{x}}_s] = \left|\mathcal{F}[\boldsymbol{x}_m]\right| \cdot \exp\left(j \cdot \angle(\mathcal{F}[\tilde{\boldsymbol{x}}_s])\right)$ as the new starting point for the iteration. This is repeated until the phase difference between $\mathcal{W}^i_{k\ell}[\tilde{\boldsymbol{x}}_s]$ and $\mathcal{W}^i_{k\ell}[\boldsymbol{x}_s]$ becomes small. We show the results in Fig. 5. An improvement can be clearly seen between the reconstructed image resulted by [12] (Fig. 5 c) and the one obtained by our proposed algorithm (Fig. 5 d).

5 Conclusions

We investigated two-dimensional CSMFBs for motion-field estimation and motion correction. We showed that the motion information is only coded by the phase information of the two-dimensional CSMFB, which significantly facilitates the motion estimation and correction. Furthermore, given a motion field, the motion can be corrected without the need for an external interpolation function. Because of this, we do not need to perform a regridding from images.

Our experimental results on the Yosemite sequence are promising, and further optimization may improve the performance on motion estimation. The main application area of the transform is seen as a building block within image reconstruction methods for capturing image sequences with non-rigid motion, such as in magnetic resonance imaging, where a k-space is corrupted.

References

1. Austvoll, I.: A study of the yosemite sequence used as a test sequence for estimation of optical flow. In: Kalviainen, H., Parkkinen, J., Kaarna, A. (eds.) SCIA 2005. LNCS, vol. 3540, pp. 659–668. Springer, Heidelberg (2005)
2. Bayram, I., Selesnick, I.W.: On the dual-tree complex wavelet packet and m -band transforms. IEEE Transactions on Signal Processing **56**(6), 2298–2310 (2008)
3. Chaux, C., Duval, L., Pesquet, J.C.: Image analysis using a dual-tree m-band wavelet transform. IEEE Transactions on Image Processing **15**(8), 2397–2412 (2006)
4. Fleet, D.J., Jepson, A.D.: Computation of component image velocity from local phase information. International Journal of Computer Vision **5**(1), 77–104 (1990)
5. Goldstein, T., Osher, S.: The split bregman method for L1-regularized problems. SIAM Journal on Imaging Sciences **2**(2), 323–343 (2009)

6. Horn, B.K.P., Schunck, B.G.: Determining optical flow. Artificial Intelligence **17**(1–3), 185–203 (1981)
7. Kyochi, S., Suzuki, T., Tanaka, Y.: A directional and shift-invariant transform based on m-channel rational-valued cosine-sine modulated filter banks. In: Proc. Asia-Pacific Signal Information Processing Association Annual Summit and Conference, Hollywood, California, pp. 1–4, December 2012
8. Kyochi, S., Uto, T., Ikehara, M.: Dual-tree complex wavelet transform arising from cosine-sine modulated filter banks. In: Proc. IEEE International Symposium on Circuits and Systems, Taipei, Taiwan, pp. 2189–2192, May 2009
9. Lu, J., Liou, M.L.: A simple and efficient search algorithm for block-matching motion estimation. IEEE Transactions on Circuits and Systems for Video Technology **7**(2), 429–433 (1997)
10. Maaß, M., Phan, H., Mertins, A.: Design of cosine-sine modulated filter banks without dc leakage. In: Proc. International Conference on Digital Signal Processing, Hong Kong, China, pp. 486–491, August 2014
11. Magarey, J., Kingsbury, N.G.: Motion estimation using a complex-valued wavelet transform. IEEE Transactions on Signal Processing **46**(4), 1069–1084 (1998)
12. Möller, A., Maaß, M., Mertins, A.: Blind sparse motion MRI with linear subpixel interpolation. In: Handels, H., Deserno, T.M., Meinzer, H.P., Tolxdorff, T. (eds.) Bildverarbeitung für die Medizin 2015. Informatik aktuell, pp. 510–515. Springer, Heidelberg (2015)
13. Mota, C., Stuke, I., Aach, T., Barth, E.: Divide-and-conquer strategies for estimating multiple transparent motions. In: Jähne, B., Mester, R., Barth, E., Scharr, H. (eds.) IWCM 2004. LNCS, vol. 3417, pp. 66–77. Springer, Heidelberg (2007)
14. Selesnick, I.W., Baraniuk, R.G., Kingsbury, N.G.: The dual-tree complex wavelet transform. IEEE Signal Processing Magazine **22**(6), 123–151 (2005)
15. Torr, P.H.S., Zisserman, A.: Feature based methods for structure and motion estimation. In: Triggs, B., Zisserman, A., Szeliski, R. (eds.) ICCV-WS 1999. LNCS, vol. 1883, pp. 278–294. Springer, Heidelberg (2000)
16. Viholainen, A., Alhava, J., Renfors, M.: Implementation of parallel cosine and sine modulated filter banks for equalized transmultiplexer systems. In: Proc. IEEE International Conference on Acoustics, Speech, and Signal Processing, vol. 6, Salt Lake City, Utah, pp. 3625–3628, May 2001
17. Viholainen, A., Stitz, T.H., Alhava, J., Ihalainen, T., Renfors, M.: Complex modulated critically sampled filter banks based on cosine and sine modulation. In: Proc. IEEE International Symposium on Circuits and Systems, vol. 1, Scottsdale, Arizona, pp. I-833–I-836, May 2002
18. Yang, Z., Zhang, C., Xie, L.: Sparse MRI for motion correction. In: Proc. IEEE International Symposium on Biomedical Imaging, San Francisco, California, pp. 962–965, April 2013